Astronomy & Astrophysics manuscript no. saxj2103˙paper
March 6, 2007

Long-term pulse profile study of the Be/X-ray pulsar SAX J2103.5+4545

A. Camero Arranz[1], C.A. Wilson[2], M.H. Finger[3], and V. Reglero[1]

[1] GACE, Instituto de Ciencias de los Materiales, Universidad de Valencia, P.O. Box 20085, 46071 Valencia, Spain
[2] NASA Marshall Space Flight Center, Huntsville, AL 35812, USA
[3] National Space Science Technology Center, Huntsville, AL 35805, USA
[3] Universities Space Research Association, Huntsville, AL 35805, USA

Received ; accepted

ABSTRACT

Aims. We present the first long-term pulse profile study of the X-ray pulsar SAX J2103.5+4545. Our main goal is to study the pulse shape correlation either with luminosity, time or energy.
Methods. This Be/X-ray binary system was observed from 1999 to 2004 by *RXTE* PCA, and by *INTEGRAL* from 2002 to 2005, during the Performance and Verification (PV) phase and the Galactic Plane Scan survey (GPS). X-ray pulse profiles were obtained in different energy ranges. The long-term spectral variability of this source is studied. The long-term flux, frequency and spin-up rate histories are computed. A new set of orbital parameters are also determined.
Results. The pulse shape is complex and highly variable either with time or luminosity. However, an energy dependence pattern was found. Single, double, triple or even quadruple peaks pulse profile structure was obtained. It was confirmed that SAX J2103.5+4545 becomes harder when the flux is higher. The new orbital solution obtained is: P_{orb}= 12.66528±0.00051 days, e = 0.401±0.018, ω = 241.36±2.18 and $a_x \sin i$ = 80.81±0.67 lt-s.

Key words. X–rays: binaries - stars: pulsars - stars: individual: SAX J2103.5+4545

1. INTRODUCTION

SAX J2103.5+4545 is a Be High Mass X-ray Binary pulsar with an orbital period of 12.68 d (the shortest known in Be/X-ray binary systems) and X-ray pulsations of 358 s. These systems consist of a neutron star orbiting a Be companion, hence forming a Be/X-ray binary. Be stars are rapidly rotating objects with a quasi-Keplerian disk around their equator. The optical and infrared emission is dominated by the donor star and its equatorial disk, and it is characterized by spectral lines in emission (particularly those of the Balmer series) and IR excess. The standard model of a Be/X-ray binary ascribes the high-energy radiation to an accreting mechanism that takes place when the compact object interacts with the Be star's circumstellar disk, giving rise to an X-ray outburst.

This source was discovered using the *BeppoSAX* satellite (Hulleman et al. 1998). The X–ray spectrum (2–25 keV) was fitted by a power-law with a photon index of 1.27±0.14 plus a photoelectric absorption at lower energies (N_H=3.1×10^{22} cm^{-2}). The likely optical counterpart is a B0Ve star (V = 14.2) at a distance of 6.5 kpc (Reig et al. 2004). Using *XMM-Newton* data a quasi-periodic oscillation at 22.7 s was discovered by İnam et al. (2004). Baykal et al. (2002) found a correlation between spin-up rate and X–ray flux during the 1999 outburst. This suggests the formation of an accretion disk during periastron passage of the neutron star. However, SAX J2103.5+4545 does not follow the Corbet P_{orb}/P_{spin} correlation found in other accreting pulsar systems.

Previously, this source has been analyzed by Hulleman et al. (*BeppoSAX*, 1998), Baykal et al. & İnam et al. (*RXTE*, *XMM-Newton*, 2000, 2004, 2007), Reig et al. (optical & IR wavelengths, 2004, 2005), Filippova et al. (optical wavelength; *RXTE*, *XMM-Newton*, *INTEGRAL*, 2004), Blay et al., Falanga et al. and Sidoli et al. only with *INTEGRAL* data (2004, 2005, 2005, respectively), Blay (optical/X-ray correlation; *INTEGRAL* 2006) and Camero-Arranz et al. 2006 with *RXTE* & *INTEGRAL* .

We present a long-term pulse profile study, as well as a spectral and pulse-timing analysis of SAX J2103.5+4545 using data from both *INTEGRAL* and *RXTE* missions.

2. OBSERVATION AND DATA REDUCTION

The **INTE**rnational **G**amma-**R**ay **A**strophysics **L**aboratory (*INTEGRAL*, Winkler et al. 2003) consists of three coded mask telescopes, the spectrometer SPI (20 keV–8 MeV), the imager IBIS (15 keV–10 MeV), and the X-ray monitor JEM-X (4–35 keV), as well as the optical monitoring camera OMC (V, 500–600nm).

SAX J2103.5+4545 has been detected by IBIS/ISGRI during *INTEGRAL* PV phase and the GPS survey from 2002 to 2005 (MJD 52618 – MJD 53356), with a total observing time of ∼860 ks. *INTEGRAL* data reduction was carried out with the Offline Scientific Analysis software, release 5.0, distributed by the ISDC (Courvoisier et al. 2003). A software description can be found in Goldwurm et al. (2003), Diehl et al. (2003), Wetergaard et al. (2003).

Send offprint requests to: A. Camero Arranz
e-mail: Ascension.Camero@uv.es

Table 1. Pulse Period detections of SAX J2103.5+4545 with IBIS/ISGRI. The second column shows the number of ScWs used for the computation in each epoch.

Epoch (MJD)	number of ScWs	Pulse Period (s)
52619.299	6	–
52630.755	49	354.927 ±0.014
52637.303	18	–
52722.884	3	354.072±0.014
52761.947	35	353.478±0.017
52797.040	2	–
52805.978	3	–
52820.945	2	–
53021.331	74	–
53038.548	119	352.446±0.019
53041.996	21	–
53102.514	3	–
53130.288	77	352.350±0.006
53133.176	51	352.29±0.01
53188.993	2	–
53258.517	3	–
53333.056	6	–
53349.280	5	–
53354.965	4	–

RXTE (Bradt et al. 1993) carries 3 instruments on board. The Proportional Counter Array (PCA; Jahoda et al. 1996) is sensitive from 2–60 keV. The High Energy X-ray Timing Experiment (HEXTE; Gruber et al. 1996) extends the X-ray sensitivity up to 200 keV. Monitoring the long-term behavior of some of the brightest X-ray sources, the All Sky Monitor (ASM; Levine et al.1996) scans most of the sky every 1.5 hours at 2–10 keV.

SAX J2103.5+4545 was also observed with *RXTE* PCA and HEXTE from 1999 to 2004 (MJD 51512.8 – MJD 53047.9), with a total observing time of ∼1900 ks. However, it is important to note that during that period there were two gaps with no observations taken by those instruments (MJD 51900 – MJD 52000 and MJD 52025 – MJD 52430). For each available observation, we have analyzed PCA Standard1 data (0.125 s time resolution, no energy resolution) for the light curves and Standard2 data (16 s time resolution, 129 channel energy resolution) for spectral analysis using FTOOLs V6.0.5. In addition, GoodXenon PCA data were selected for the pulse profile study, and HEXTE binned mode data from clusters A and B for the spectral analysis.

3. DATA ANALYSIS AND RESULTS

3.1. PULSE PROFILE

In order to study the long-term pulse profile dependence on luminosity, time or orbital phase we extracted 548 *RXTE* PCA Standard1 light curves in the 2–60 keV energy range. The background was not subtracted in this first step. Then, we corrected the times to the barycenter of the solar system, as well as for the orbital motion using the binary orbital parameters by Baykal et al. (2002). We constructed pulse profiles by fitting the data with a harmonic expansion in pulse phase (6 harmonics were used). Typically we use data spanning a 4000 s interval (∼11 pulse periods). Initially

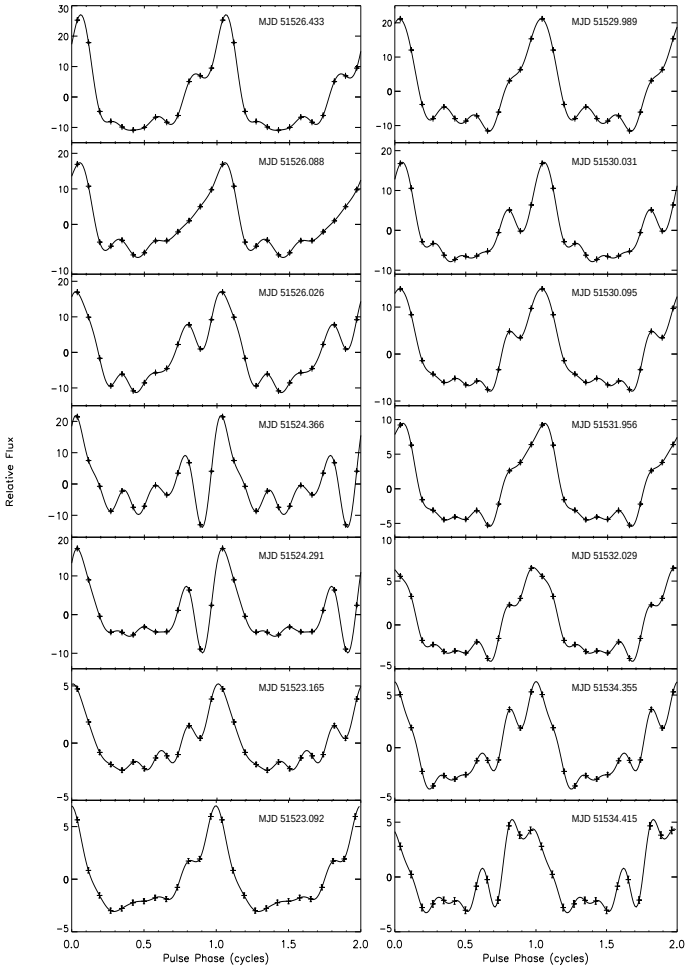

Fig. 1. *RXTE* PCA (2–60 keV) pulse profiles consecutive in time during outburst. Two cycles are plotted for clarity. The evolution on intensity of the first part of the outburst is plotted on the left column increasing from bottom to top. The fall is plotted on the right, with intensity decreasing from top to bottom.

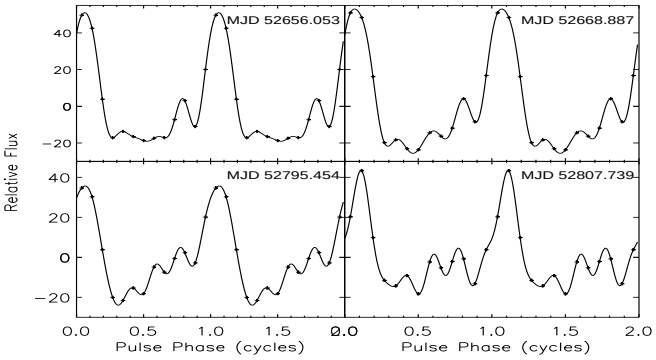

Fig. 2. PCA (2–60 keV) pulse profiles at the same orbital phase (0.73±0.02 cycles) and at the same luminosity state ($5.62\pm0.04\times10^{+36}$ erg s^{-1}).

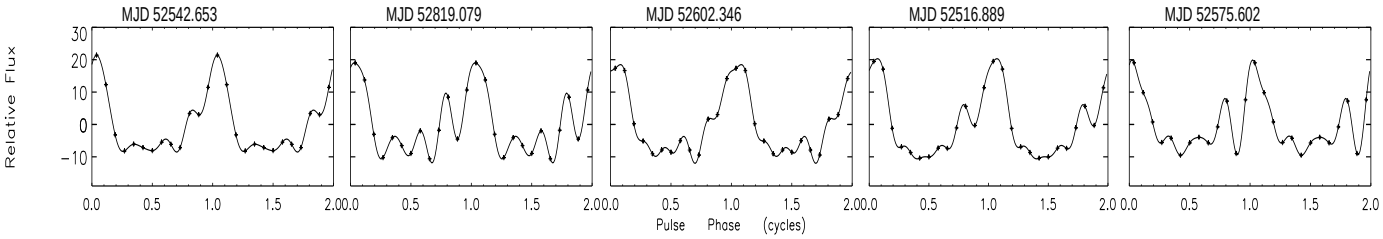

Fig. 3. *RXTE* PCA 2–60 keV pulse profiles at the same luminosity state (L = $2\pm0.6\times10^{+36}$ erg s^{-1}).

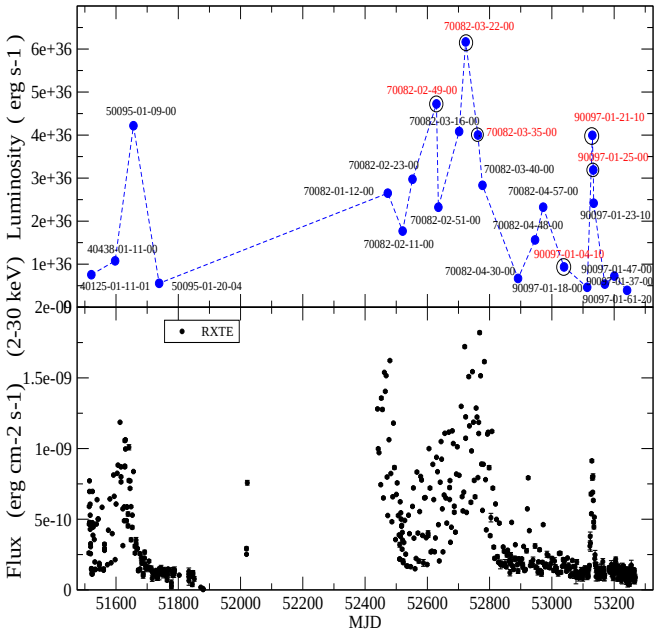

Fig. 4. Top. Sample of PCA observations selected for the pulse profile intensity analysis. An extra circle indicates the existence in addition of an *INTEGRAL* IBIS/ISGRI observation. Bottom. *RXTE* PCA flux in the 2-30 keV energy range.

we used a simple phase model ($\phi(t_k)= \phi_o+f_o(t_k-t_o)$; where f_o is the pulse frequency at time t_o and ϕ_o is the phase at time t_o). The errors on the Fourier coefficients were corrected for the non-Poisson noise found in the power spectra (Wilson et al. 2002). In a later stage, a more precise quadratic-spline phase model was created, which was used to remake the profiles.

Taking consecutive pulse profiles in time during outbursts, we found a non correlated shape pattern from one outburst to another, and even different patterns either going up or down for a given outburst (see Fig. 1, where Relative Flux is the number of counts per second and per PCU relative to the mean rate). In general, the shapes vary from a strong single sinusoidal-like peak to double. However, three or even four weaker peaks are often found in addition to the main one. This source showed the same arbitrary conduct sorting the profiles by orbital phase (see Fig. 2). Moreover, we expected to obtain a base profile for a given X–ray luminosity. Nevertheless, we discovered a diversified range of shapes with no clear resemblance (see Fig. 3).

Once we realized that no temporal, orbital or luminosity correlations were found in the original PCA data sample in the 2-60 keV range, we decided to select only 24 goodXenon *RXTE* PCA observations for the energy dependence study. The chosen data set follows the long-term light curve behavior and covers MJD 51512.8 to 53047.9 (see Fig. 4). The PCA background subtracted light curves were obtained in four energy ranges: 2.06–5.31 keV, 5.31–7.76 keV, 7.76–13.93 keV, 13.93–20.62 keV. Then, the same procedure was followed to construct the phases and then the profiles, as we described before. Typically, the duration of a *RXTE* PCA observation is about 3000 s and the profiles contain about 8 pulse cycles. To complete this study, we obtained a list of good events times per science window (ScW) with IBIS/ISGRI in the 20–60 keV energy band. Table 1 shows a summary of the detections and non detections with this instrument, as well as the number of ScWs used for making profiles. In Figure 4 we marked on red (and an extra circle) those 6 points in which we also have an IBIS/ISGRI positive detection.

Figures 5 and 6 show the evolution of some of the PCA profiles in four energy bands (with energy increasing from top to bottom). As we already mentioned, the profiles present a prominent sinusoidal-like peak among other features. These can vary from one to three peaks in addition to the main one. The general behavior is:

1. The right side of the main peak (phases 0.0–0.2) remains quite similar as energy increases.

2. The region at phases 0.2–0.5 tends to fill as energy increases. It is not always a peak.

3. When a peak is present at phases 0.5–0.7, the larger is the energy the weaker is the feature.

4. At phases 0.7 to 0.9 a secondary peak or shoulder is present. It gets smaller with increasing energy.

5. The dip in the mean peak (phase 0.9) becomes deeper as the flux increases. The maximum depth is found in the 7.76–13.93 keV band, and then decreases again with energy. In particular, observations 70082-03-16-00 and 70082-04-57-00 show this notch especially deep and wide, evolving the last one to a strong double peak (see Fig. 5 and 6).

This trend is also seen in the 20–60 keV IBIS/ISGRI profiles (see Fig. 7), where the second and the third peaks are almost missing and the fourth one is stronger, but still weaker than the mean peak.

3.2. SPECTRAL ANALYSIS

We have obtained 548 spectra from 6 years of *RXTE* PCA and HEXTE data (MJD 51512.8 – MJD 53047.9). For each observation, we have selected PCA Standard2 data and HEXTE binned mode data from clusters A and B. Then, fluxes in all the different energy ranges were obtained by fitting a cut-off power law model plus a photoelectric absorption (phabs×(gauss + cutoffpl)) to each 2.7–70 keV spectrum, fixing the iron line value

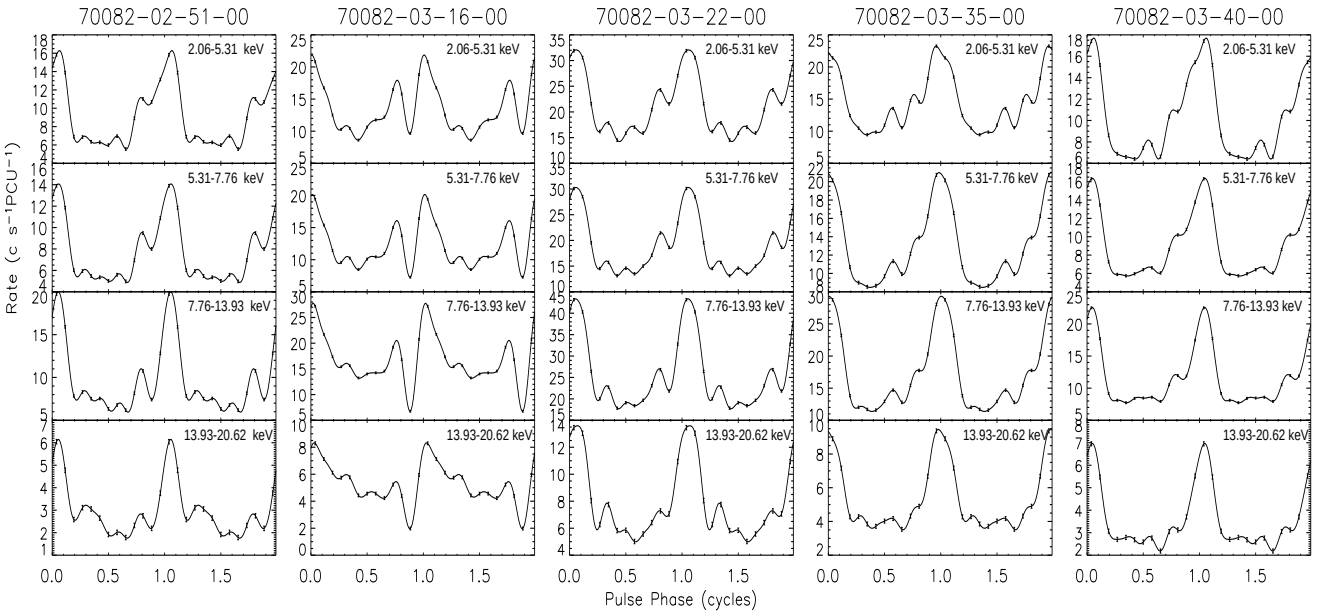

Fig. 5. Evolution of SAX J2103.5+4545 PCA pulse profile with intensity in 4 energy bands (from top to bottom). They are sorted consecutive in time during the brightest period (MJD 52650–52800) of the source.

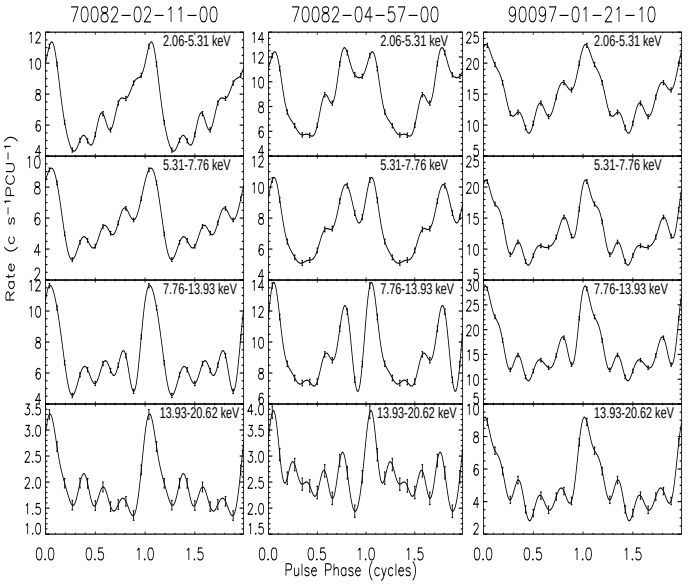

Fig. 6. Some examples of SAX J2103.5+4545 PCA pulse profiles showing a more complex structure, in the same 4 energy bands.

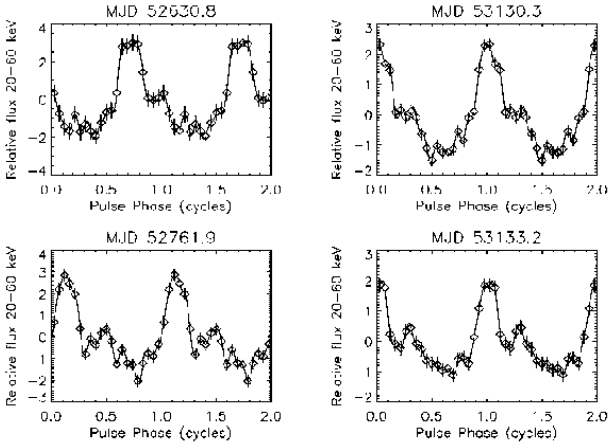

Fig. 7. ISGRI (20-60 keV) mean pulse profiles of SAX J2103.5+4545 generated by combining profiles from individual *INTEGRAL* ScWs.

and its width to 6.43 keV and 0.165, respectively (Baykal et al. 2002). They were also background subtracted.

In fig. 9 (bottom) we show the long-term flux history of SAX J2103.5+4545 using *RXTE* and *INTEGRAL* data, which follows very nicely the general trend of the long-term frequency derivatives history obtained after the timing analysis (see next section).

To study the spectral variability of SAX J2103.5+4545 we have computed the long-term hardness ratios (HR) using two energy bands: 2–10 keV, 10–30 keV (defined as $HR = H/S$). Figure 8 (top) shows an average of the calculated HR vs. time and intensity, using those energy bands. In the HR vs. intensity plot we took out few detections corresponding to the faintest state, due to their enormous error bars, which hid the general trend. The correlation between the HR either with time or intensity is clear. We can see that the source becomes harder when the flux is higher. In the same figure we have included some plots showing the evolution of the absorption, the Photon Index, the cutoff and the reduced χ^2 with intensity. We have also rejected the faintest flux values since the uncertainties obtained in the parameters were very large, adding only confusion to the study. We found variable behavior just in the Photon Index vs. intensity plot. The larger is the flux the lower is the the photon index. This anti-correlation was the expected and shows again that in the bright state the spectrum of SAX J2103.5+4545 is harder than in the faint state. It is

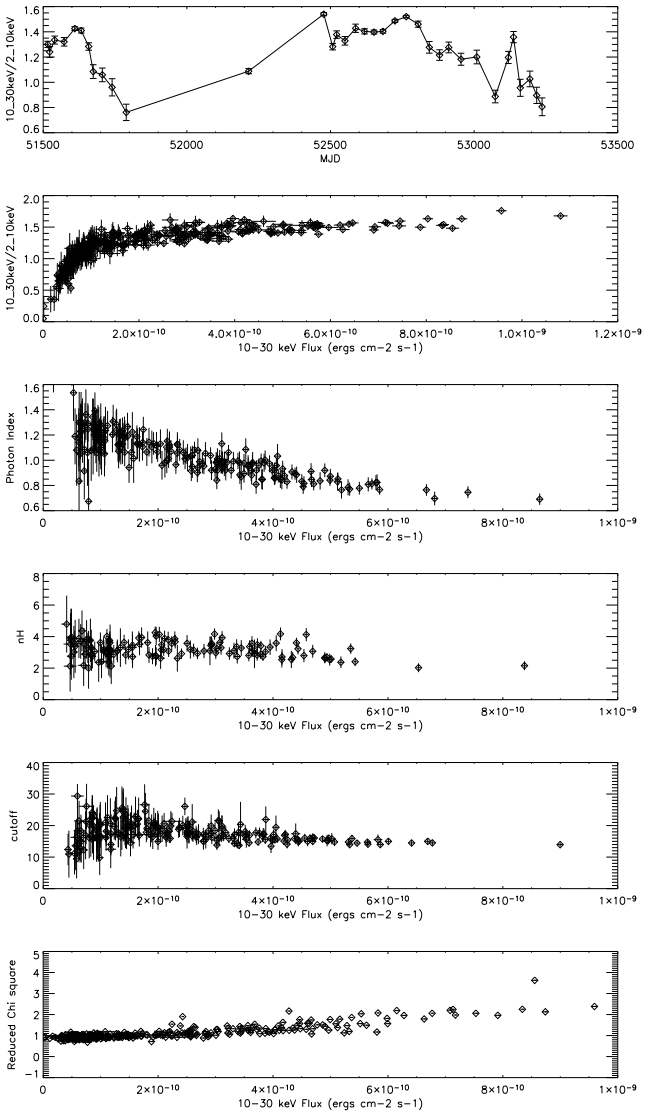

Fig. 8. Top. Long-term Hardness ratios history. From middle to bottom: HR-intensity diagram and spectral parameters evolution vs. intensity.

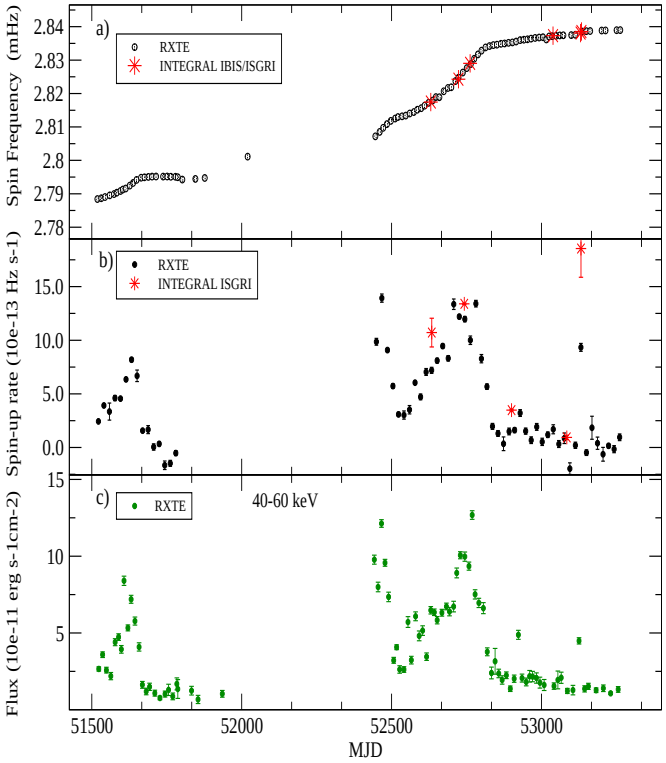

Fig. 9. Top: Long-term frequency history. Middle: Averaged spin-up rates history. Bottom: 40-60 keV *RXTE* HEXTE averaged fluxes. A spin-up rate and X–ray flux correlation was found, confirming that an accretion disk during periastron passage is present.

clear that the fitting model applied is not the perfect one for the bright state, as we can see in the reduced χ^2 vs. intensity figure. Nevertheless, it was found to be the best simple model for all the ∼500 spectra analyzed. Baykal et. al (2007) suggested that this type of spectral softening with decreasing flux was found to be mainly a consequence of mass accretion rate change and was not necessary to be related to a significant accretion geometry change.

3.3. TIMING ANALYSIS

3.3.1. Phasing

We selected again the 548 *RXTE* PCA observations for the long-term timing analysis. Then we obtained either a list of good events times per science window (*INTEGRAL* IBIS/ISGRI, 20–60 keV) or binned light curves (*RXTE* PCA, 2–60 keV). The times were corrected to the barycenter of the solar system and for the orbital motion. We constructed pulse profiles in those energy bands by fitting the data with a harmonic expansion in pulse phase, as we described in the Pulse Profile section. Initially we used the same simple phase model and the errors on the Fourier coefficients were corrected for the non-Poisson noise.

The profiles were grouped into 12.69 d intervals with frequencies and frequencies derivatives being estimated for each interval using a grid search of the Y_n statistics (Finger et al. 1999). The measured frequencies were then fitted with a piecewise-linear model. Then the profiles were remade using the integral of the fitted frequency model as a phase model.

For the *INTEGRAL* IBIS/ISGRI data the approach was different, due to the non continuous observational pattern and the sensitivity of the ISGRI detector (see Table 1). A template profile was then created from the average profile from the set of ISGRI ScWs and from the collected pulse profiles from the *RXTE* PCA data. To generate phase offsets from the model, we then cross-correlated the individual profiles with the template profiles. The new phases (model + offset) were then fitted with a quadratic-spine phase model, which was used to remake the profiles. New phase offsets were then estimated.

Figure 9 shows the long-term spin-frequency and spin-up rate history obtained after repeating the grid search with the new profiles and phases. For IBIS/ISGRI the spin rates were computed by differencing adjacent frequency measurements and dividing by the corresponding time difference. The PCA spin rates were computed by fitting a quadratic function to the phases, which were divided in 29 time intervals. We see that the first outburst of SAX J2103.5+4545 started with a spin-up trend (bright

Table 2. Orbital solution for SAX J2103.5+4545.

	Baykal et al. (2002)	İnam et al. (2004)	Sidoli et al. (2005)	Baykal et al. (2007)	Present work
$T_{pi/2}$ (MJD)	51519.3±0.2	52633.90±0.05		52469.336±0.057	52545.411±0.024
P_{orb} (days)	12.68±0.25		12.670±0.005	12.66536±0.00088	12.66528±0.00051
$a_x \sin i$ (lt-s)	72±6			74.07±0.86	80.81±0.67
e	0.4±0.2			0.4055±0.0032	0.401±0.018
ω	240±30			244.3±6.0	241.36±2.18

state), made a transition to a steady spin rate (faint state), and then appeared to just begin a spin-down trend. The following available data started with a quick spin-up trend (bright state), and then a transition to a slower spin-up rate (faint state).

Comparing the fluxes obtained in the non averaged long–term light curve (the one composed of around 500 individual flux measurements from the spectra; see bottom of fig. 4), we realized that while SAX J2103.5+4545 was in the faint state (MJD 53100), suddenly it increased dramatically its luminosity for a short time period. This was not the first episode of such a behavior but the strongest one. Therefore, the ISGRI frequency derivative outlier cannot be ruled out since it seems it is related to a significant event.

3.3.2. Orbit fitting

Errors in the orbital parameters caused by coupling between the intrinsic spin variations of the pulsar with orbital effects, can scatter the detected pulse frequencies. In order to achieve a better characterization of the geometry of this binary system, we have used *RXTE* PCA Standard1 data to obtain a new set of orbital parameters. To take into account the phase noise caused for pulse profiles variations we split the *RXTE* results into 29 intervals (3 orbits) and fit an orbit to the phases in each interval (the orbital Period was fixed). The fitting model for each interval consisted of a orbital model, a quadratic-phase model.

The final orbital parameters were obtained from a weighted average of the best fit parameters from just 28 intervals. As we mentioned above, taking a look at the long-term light curve we noticed that around MJD 53100 took place a huge and narrow spike while the source was in the faint state. This surprisingly behavior was also noticed in the orbital fit number 26, obtaining a highly dispersed fit that was finally rejected. The final orbital epoch and period were obtained by making a linear fit to the 28 best fit orbital epochs. The errors in these parameters were estimated from the scatter of the best fit parameters. Table 2 lists the final orbital parameters obtained for the combined fit, where $T_{pi/2}$ is the epoch when the mean orbital longitude is equal to 90 deg, P_{orb} is the orbital period, $a_x \sin i/c$ is the light-travel time for the projected semi-major axis (i is the inclination angle), e is the eccentricity and ω is the longitude of periastron.

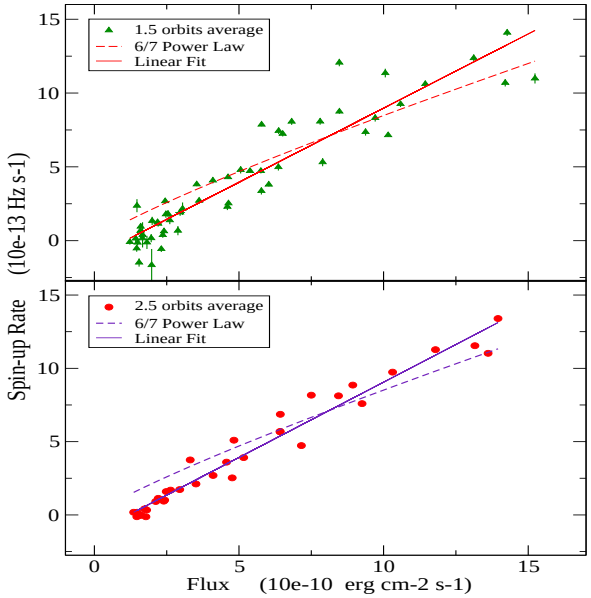

Fig. 10. Spin-up rates vs. *RXTE* 2–100 keV non absorbed averaged Flux every 1.5 and 2.5 orbits. A linear fit was found the best one.

3.3.3. Spin-up Torque-Flux correlations

We averaged the non absorbed flux every 1.5 and 2.5 pulsar orbits. The 1.5 orbits average is the smallest time interval that allowed us to fit a quadratic function to the phases when the spin rates were computed. The second time interval of 2.5 orbits was chosen as a good representative of the general trend. Fig. 10 shows more clearly the spin-up rate vs. flux correlation, with a linear correlation coefficient of 0.94 and 0.98, respectively. When we fitted both data sets with a single power law (*solid line*), we obtained for the best fit slopes of (1.005–1.027)±(0.05–0.035)×10^{-3} erg cm^{-2} and an x-intercept (2–100 keV non absorbed flux at zero spin-up) of (-1.07–(-1.21))±(0.32–0.22)×10^{-10} ergs cm^{-2} s^{-1}. Both results are coherent. They are identical within errors, however it is interesting to note that data averaging over 1.5 orbits scatters more than averaging over 2.5 orbits. It appears that the smaller is the average the bigger is the scattering. This might suggest that, in addition to the disk accretion mechanism, there seems to exist another mechanism producing erratic variations.

In the same figure, a dashed line denotes our best-fit power law with an index fixed at 6/7, which represents the

relationship between spin-up and flux predicted by simple accretion theory. We can see that this fit does not match totally the observed behavior. It suggests that a more sophisticated model, e.g. Ghosh and Lamb, as in Baykal et al. (2007), seems to be needed at low-flux end, because the pulsar is beginning to spin-down. At the high-energy flux end, beaming may be boosting the observed flux.

4. DISCUSSION

4.1. NATURE OF THE SOURCE

Some X–ray pulsars, like EXO 2030+375 (Parmar et al., 1989), show a clear pulse shape dependence on source luminosity, most likely controlled by accretion rate. Differences in X–ray pulse profiles are considered to be due to the differences in the geometrical configuration with respect to the rotational axis of the neutron star, the axis of magnetic dipole moment, and the observer's line of sight (Nagase 1989). The structure of the accretion column determines the basic profile of the pulse pattern. However, simple geometric models with two pencil beams coming from the magnetic poles or two bright spots on the neutron star surface, cannot explain the variability observed in some other systems, like Vela X–1. Previous studies by Kreykenbohm et al. (2002) confirmed for that system a very complex pulse profile at low energies (below 6 keV), showing a five peak structure. Above 10 keV the pulse profiles evolved into a simple double peak. They pointed out that a good description of the processes responsible for the complex shape at low energies is still missing.

In the present work, the 2–60 keV SAX J2103.5+4545 pulse profiles obtained with *RXTE* PCA were found to be peculiarly complex and variable either with luminosity, time or orbital phase. For the first time the pulse shapes seem to vary randomly from not only single sinusoidal-like peak but profiles with two, tree and even occasionally four peaks, with no evident interrelationship. For a given energy range, temporal variability of the pulse profile of SAX J2103.5+4545 was explained by Sidoli et al. (2005) likely due to time-dependent emission pattern, or to changes in the opacity of the magnetized plasma where the radiation propagates.

Previous works by Baykal et al. (2002), Falanga et al. and Sidoli et al. (2005) obtained a single peak pulse profile in soft X–ray bands, using *RXTE* and *INTEGRAL* data. However, İnam et al. (2004) found a double peak profile using *XMM-Newton*. Although this seem not to be in agreement, could be compatible due to the variability seen in our study for SAX J2103.5+4545.

In the hard X–ray range, we have obtained much more simple 20–40 keV *INTEGRAL* ISGRI profiles. In particular, double-like peak profiles in agreement with previous results by Falanga et al. and Sidoli et al. (2005). Filippova et al. (2004) published a 20–100 keV single peak pulse profile using PV phase *INTEGRAL* data. This result might be in agreement with our PV phase results, taking into account their uncertainties.

In addition, our study allowed us to confirm an energy dependence pattern for SAX J2103.5+4545. Unfortunately, as in Vela X–1, we did not find out a straightforward explanation for the low energy pulse profiles. İnam et al. (2004) found practically no variation in the energy dependence of the 0.9–11 keV pulse profiles, which is not in agreement with our results. Falanga et al. (2005) obtained an energy dependent secondary peak around phase 0.2, which became more evident at energies above 20 keV. This peak might be compatible with the trend of our peak at phase 0.7. They also claimed that at phase 0.6 hick-ups were present, in agreement with those observed by İnam et al. (2004) using *XMM-Newton* data. These hick-ups were only visible at high energies (40–80 keV). Again, these features might be compatible with our dip at phase 0.9.

It is generally accepted that in order to explain the energy-dependent changes of the pulse profile, the anisotropic radiation transfer must be taken into account (Nagase 1989). Previous studies by Krauss et al. (2003) found that energy-dependent peaks in medium luminosity binary X–ray pulsars, are mainly due to energy-dependent relative importance of the halo (which forms around the accretion funnel where the neutron star surface is irradiated) and the column contributions to the observed flux (Sidoli et al. 2005). For SAX J2103.5+4545, Falanga et al. (2005) found that changes in the morphology of the pulse profile as a function of energy were consistent with variations in the spectral components visible in their pulse phase resolved spectra analysis. Their study also showed that differences in the double-peak can be modeled by a different scattering fraction between the radiation from the two magnetic poles.

First studies of SAX J2103.5+4545 by Baykal et al. (2002) showed a transition from spin-up to spin-down in the *RXTE* observations from an outburst in November 1999, suggesting the presence of an accretion disk. The detection of a quasi-periodic oscillation at 22.7 s discovered by İnam et al. in 2004, provided further evidence for this existence. The spin-up rate and X-ray flux correlation is also observed in the present work, confirming that an accretion disk is present during periastron passage. Previous works by İnam et al. (2004) and Baykal et al. (2002, 2007) are in good agreement with our results. In general, either the pulse period estimations from Sidoli et al. (2005) or those ones from Blay et al. (2006) are not in very good agreement with our results.

It is frequently assumed that in normal outbursts no disk forms around the neutron star and accretion is directly from the disk-like outflow from the Be star, so significant spin-up is not expected because direct wind accretion is not believed to be very efficient at transferring angular momentum (Wilson et al. 2002, and references therein). If enough angular momentum is present in the accreted material, an accretion disk will form. However, evidence for spin-up during normal outbursts has been observed in GS 0834-430 (Wilson et al. 1997), 2S 1417-624 (Finger, Wilson & Chakrabarty 1996), 2S 1845-024 (Finger et al. 1999), and in EXO 2030+375 (Stollberg et al. 1999; Wilson et al. 2002, 2005).

Simple accretion theory assumes that the material from the companion star is flowing onto a rotating neutron star with a strong magnetic field. This field determines the motion of material in a region of space called the magnetosphere. The size of this region is denoted by the magnetospheric radius r_m, given by (Pringle & Rees 1972; Lamb, Pethick & Pines 1973)

$$r_m \simeq k(GM)^{-1/7}\mu^{4/7}\dot{M}^{-2/7} \quad (1)$$

where G is the gravitational constant, k is a constant factor of order 1, M is the mass of the neutron star, and $\dot{M}$ is the mass accretion rate: $\dot{M} = 4\pi d^2 FR/GM$ (where R is the radius of the neutron star and d is the distance to the pulsar). Equation (1) with $k \simeq 0.91$ gives the Alfvén radius for spherical accretion and with $k \simeq 0.47n(\omega_s)$ gives the magnetospheric radius derived by Ghosh & Lamb (1979).

The torque applied by accretion of matter onto a neutron star, assuming torques due to matter leaving the system are negligible, is given by (Lamb, Pethick & Pines 1973)

$$\frac{d}{dt}(2\pi I\nu) = \dot{M}\ell \tag{2}$$

where I is the moment of inertia of the neutron star and ℓ is the specific angular momentum of the material. If I is assumed constant, then ℓ is given by

$$\ell = 2\pi I\dot{\nu}\dot{M}^{-1} \tag{3}$$

where $\dot{\nu}$ is the spin-up rate. To estimate ℓ for SAX J2103.5+4545, we assumed typical pulsar parameters, $M = 1.4\ M_\odot$, $R = 10$ km, $I = 10^{45}$ g cm^2, typical values of $\dot{\nu} \simeq 7 \times 10^{-13}$ Hz s^{-1}, $F \simeq 7 \times 10^{-10}$ erg cm^{-2} s^{-1} (see Fig. 10). The distance of the source from optical observations is 6.5 ±0.9 kpc (Reig et al., 2004, 2005). Several authors have discussed a possible value for the magnetic field. Recently, Baykal et al. (2007) obtained a value of 16.5×10^{12} Gauss. But this implied a distance of 4.5 kpc. In order to explain the spin-up rate observed, and assuming that the distance of 6.5 kpc is correct, Sidoli et al. (2005) obtained a magnetic field of $\sim 1.6\times10^{12}$ Gauss. No cyclotron lines have been observed from this source. One explanation could be a high magnetic field as proposed by Baykal et al. (2007) which would imply a fundamental line at ∼200 keV.

An accretion disk will form if the specific angular momentum of the material accreted from the Be star's disk is comparable to the Keplerian specific angular momentum at the magnetospheric radius, i.e.

$$\ell \simeq \ell_m = (GMr_m)^{1/2} \tag{4}$$

For SAX J2103.5+4545, we have summarized in Tab. 3 the different values obtained forℓ, using the two magnetic field measurements discussed above, assuming two distance values of 6.5 kpc and 4.5 kpc, and for $k = 0.91$ and 0.47. All the cases suggest that a disk is likely present. Only those cases which lower ℓ/ℓ_m might indicate that periods of wind accretion and disk accretion could also take place in this system.

In contrast, for the wind-fed system Vela X–1 where a disk is not expected to be present, $\dot{\nu} \simeq 6 \times 10^{-14}$ Hz s^{-1}, $L \simeq 2\times10^{38}$ ergs s^{-1}, and $\mu \simeq 2.1 \times 10^{30}$ G cm^3 leading to $\ell \simeq 0.002\ell_m$. Furthermore, three-dimensional simulations of wind accretion show that the average specific angular momentum accreted via this mechanism is always smaller than the keplerian value (Wilson et al. 2003, and references therein).

To determine whether or not centrifugal inhibition of accretion is operating, we estimated the flux at the onset of this effect by equating the magnetospheric radius to the corotation radius. The magnetospheric radius is given by equation 1, and the corotation radius is given by

$$r_{co} = (GM)^{1/3}(2\pi\nu)^{-2/3} \tag{5}$$

Table 3. Table 3. Comparison of the specific angular momentum of the accreted material to the Keplerian specific angular momentum at the magnetospheric radius. An estimation of the flux for the onset of centrifugal inhibition of accretion is also shown.

	B= 16.5×10^{12} G (4.5 – 6.5) kpc	B= 1.65×10^{12} G (4.5 – 6.5) kpc
k=0.91	ℓ= (0.61 – 0.33)ℓ_m	ℓ= (1.19 – 0.63)ℓ_m
	F_{min}*= (20.4 – 9.8)	F_{min}*= (0.2 – 0.097)
k=0.47	ℓ= (0.85 – 0.45) ℓ_m	ℓ= (1.65– 0.88) ℓ_m
	F_{min}*= (2.02 – 0.97)	F_{min}*= (0.02 – 0.0097)

* ×10^{-12} erg cm^{-2}s^{-1}

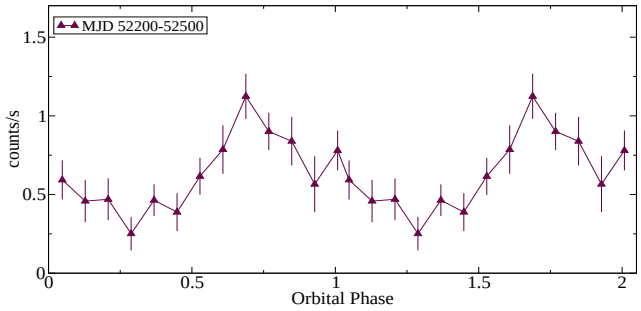

Fig. 11. *RXTE* ASM orbital light curve of SAX J2103.5+4545 from MJD 52200–52500.

where ν is the spin frequency of the pulsar. Setting $r_m = r_{co}$ gives the threshold flux for the onset of centrifugal inhibition of accretion, i.e.,

$$F_{min} \simeq 2 \times 10^{-12} ergcm^{-2}s^{-1} \times k^{7/2}{\mu_{30}}^2 {M_{1.4}}^{-2/3} {R_6}^{-1} {P_{354.9s}}^{-7/3} {d_{kpc}}^{-2} \tag{6}$$

where μ_{30}, $M_{1.4}$, R_6, and $P_{354.9}$ are the pulsar's magnetic moment in units of 10^{30} G cm^3, mass in units of $1.4M_\odot$, radius in units of 10^6 cm, and spin period in units of 354.9 s, respectively. Tab. 3 shows our measured F_{min} using equation 6. Our observed upper limit fluxes are in the range ≃ (5–0.9)×10^{-12} erg cm^{-2}s^{-1}, consistent with SAX J2103.5+4545 entering the centrifugal inhibition of accretion regime only for B= 16.5×10^{12} G (see Tab. 3).

4.2. TRANSIENT VS. PERSISTENT

Up to now, SAX J2103.5+4545 has been classified as a transient Be/X–ray binary system. However, this source is a very interesting case. A study by Reig et al. (2005) of the correlated X/optical data of this source during quiescence, showed that X–ray emission must come from stellar wind, since the source had completely lost its circumstellar disk. He also pointed out that SAX J2103.5+4545 occupies the region of the wind-fed supergiant binaries in the P_{spin}-P_{orb} diagram. Thus, in principle, accretion from the stellar wind of the BO companion might be at the origin of the observed luminosity in that state. And maybe, to be located in the wind-fed supergiant region might be also the origin of the complex SAX J2103.5+4545 pulse profile behavior.

In the present work we have not obtained observations where SAX J2103.5+4545 was not detected, hence it is

unclear how to determine outbursting vs. quiescence. Defining a threshold for the observed flux at 5×10^{-12} erg $cm^{-2}s^{-1}$, we might see 5 outbursts from Fig. 4 (bottom). Ignoring the fact that the luminosity never exceeds 10^{37} erg $cm^{-2}s^{-1}$, the first three might be qualify as type II outbursts: a) they last for multiple orbits, b) there is only moderate orbital modulation (see Fig. 11), c) there is a flux-spin up correlation. The last two outbursts are short. In the "quiescence" state where the luminosity is $\sim10^{35}$ erg $cm^{-2}s^{-1}$, we see a gradual flux decline after the third "type II" outburst, yet the frequency continues to increase. This is again not typical, but it has been seen in wind-fed systems (Bildsten et al, 1997). Overall, the behavior of the source does not fit well with the standard picture of Be/X-ray transients. We also believe that this peculiar Be/X–ray system with the narrowest orbit, may be classified as a Persistent (but highly variable) source.

Acknowledgments. We thank Peter Kretschmar for very useful comments and his support. We also appreciate to NASA Marshall Space Flight Center, the National Space Science Technology Center and the Universities Space Research Association for the opportunity to develop the present work. This research is supported by the Spanish Ministerio de Educación y Ciencia through grant-no ESP2002-04124-C03-02.

References

Baykal, A., Stark, M. J., Swank, J. H., 2000, ApJ, 544, L129
Baykal, A., Stark, M. J., Swank, J. H., 2002, ApJ, 569, 903
Baykal, A., İnam, S. ., Stark, M. J., et al. 2007, MNRAS, 374, 1108-1114
Blay, P., Reig, P., Martínez Núñez, S., Camero, A., 2004, A&A, 427,293
Blay, P. 2006. PhD thesis work: Multiwavelength Analysis of two peculiar High Mass X-ray binary systems: 4U 2206+45 and SAX J2103.5+4545. New insights from INTEGRAL.
Bradt, H. V., Rothschild, R. E., $ Swank, J. H., 1993, A&AS, 97, 355
Camero Arranz, A., Wilson, C.A., Finger, M.H., and Reglero, V. 2006, Proc. 6th *INTEGRAL* Workshop (in press)
Courvoisier, T. J.-L., Walter, R., Beckmann, V., et al. 2003, A&A, 411L, 53
Diehl, R., Baby, N., Beckmann, V., et al. 2003, A&A, 411L, 117D
Falanga, M., di Salvo, T., Burderi, L., Bonnet-Bidaud, J. M., 2005, A&A, 436, 313
Filippova, E. V., Lutovinov, A. A., Shtykovsky, P. E., et al. 2004, Astronomy Letters, 30, 12, 824
Finger, M.H., Wilson, R.B., Chakrabarty, D., et. al. 1996, A&AS, 120, 209
Finger, M.H., Bildsten, L., Chakrabarty, D., et. al. 1999, ApJ, 517, 449F
Ghosh, P., & Lamb, F.K. 1979, ApJ, 234,296
Goldwurm, A., David, P., Foschini, L., et al. 2003, A&A, 411L, 223G
Gruber, D. E., Blanco, P. R., Heindl, W. A. et al. 1996, A&AS, 120, 641
Hulleman, F., in 't Zand, J. J. M., Heise,J., 1998, A&A, 337L, 25H
İnam, S. ., Baykal, A., Swank, J., Stark, M. J., 2004, ApJ, 616, 463
Jahoda, K., Swank, J., Giles, A.B. et al. 1996, Proc. SPIE, 2808, 59
Kraus, U., Zahn, C., Weth, C., & Ruder, H., 2003, ApJ, 590, 424
Kreykenbohm, I., Coburn, W., Wilms, J., et at. 2002, A$A, 395, 129
Lamb, F. K., Pethick, C. J., & Pines, D. 1973, ApJ, 184, 271
Levine, A. M., Bradt, H., Cui, W. et al. 1996, ApJ, 469, L33
Nagase, F. 1989, Publ.Astron. Soc. Japan 41, 1
Parmar, A. N., White, N. E., Stella, L. et al. 1989, ApJ, 338, 373
Pringle, J.E., & Rees, M.J. 1972, A&A, 312,872
Reig, P., Negueruela, I., Fabregat, J., et al. 2004, A&A, 421, 673
Reig, P., Negueruela, I., Papamastorakis, G., et al. 2005, A&A, 440, 637
Sidoli, L., Mereghetti, S., Larsson, S., Chernyakova, M.,2004, Proc. 5th *INTEGRAL* Workshop (ESA SP-552), 475
Sidoli, L., Mereghetti, S., Larsson, S., Chernyakova, M., 2005, A&A, 440, 1033S
Stollberg, M.T., Finger, M.H., Wilson, R.B., et al. 1999, ApJ, 512, 313
Westergaard, N. J., Kretschmar, P., Oxborrow, C. A., et al. 2003, A&A, 411L, 257W
Wilson, C.A., Finger, M.H., Harmon B. A. et al. 1997, ApJ, 479, 388
Wilson, C.A., Finger, M.H., Coe, M.J., Laycock, S., & Fabregat, J. 2002, ApJ, 570, 287
Wilson, C.A., Finger, M.H., Coe, M.J., & Negueruela, I. 2003, ApJ, 584, 996
Wilson, C.A., Fabregat, J., Coburn, W., 2005, ApJ, 620, L99